Journal of Molecular Structure 1197 (2019) 354–360

Contents lists available at ScienceDirect

Journal of Molecular Structure

journal homepage: http://www.elsevier.com/locate/molstruc

Green synthesis of SnO_2 nanoparticle using *Lycopersicon esculentum* peel extract

H.E. Garrafa-Galvez [a], O. Nava [b], C.A. Soto-Robles [b], A.R. Vilchis-Nestor [c], A. Castro-Beltrán [a, *], P.A. Luque [b, **]

[a] Facultad de Ingeniería Mochis, UAS, C.P. 81223, Los Mochis, Sinaloa, Mexico
[b] Facultad de Ingeniería, Arquitectura y Diseño-Universidad Autónoma de Baja California, C.P. 22860, Ensenada, BC, Mexico
[c] Centro Conjunto de Investigación en Química Sustentable, UAEM-UNAM, Toluca, Mexico

ARTICLE INFO

Article history:
Received 2 March 2019
Received in revised form
9 July 2019
Accepted 11 July 2019
Available online 12 July 2019

Keywords:
Green synthesis
Lycopersicon esculentum peel extract
Tin dioxide
Methylene blue degradation

ABSTRACT

In this work, different amounts of *Lycopersicon esculentum peel extract* were used in a low cost, non-toxic green synthesis of tin dioxide nanoparticles. The generated nanoparticles presented the following characteristics: Sn-O bond at 666 cm^{-1}; crystalline growth in a purely tetragonal crystal structure; a different size and shape homogeneity, depending on the amount of extract used; and a band gap of around 3.3 eV. Of the generated nanoparticles, the sample with 4% peel extract presented a UV-light photocatalytic degradation rate of methylene blue of around 100% at 120 min; these results are better than those achieved by commercially available tin dioxide nanoparticles.

1. Introduction

The excessive use of synthetic dyes in different industries, such as textiles, cosmetics, paper, pharmaceutical and food, has brought forth a serious environmental problem due to toxic wastewater spillage into different bodies of water [1]. Synthetic dyes have generated a significant risk for living organisms, the hydrosphere, and to humans due to their toxicity and their tendency towards eutrophication [2]. Therefore, due to its complex structure, high stability and especially its low biodegradability, the elimination of synthetic dyes from toxic wastewater, before discharge, is of great importance [3]. However, several studies have been carried out for the elimination of dyes from effluents via physical, chemical, and biological methods [4], but they have presented certain disadvantages such as only a partial elimination of the dye, slow processes, the requirement of expensive equipment, and they can produce secondary pollution. Therefore, the photocatalytic method has been developed as an alternative for the degradation of dyes due to its simplicity, low toxicity, and high efficiency [5]. In recent years, metal oxide semiconductors have attracted the attention of the scientific community due to their high photocatalytic capacity under irradiation with ultraviolet light (UV) for the degradation of various environmental pollutants such as detergents, pesticides, dyes, and volatile organic compounds when treating wastewater [6]. Among the various metal oxide semiconductors, tin dioxide (SnO_2) has attracted attention due to its unique optical and electrical properties, such as low resistivity, optical transparency, and high specific theoretical capacity, as well as being an n-type semiconductor and having a wide bandwidth of 3.6 eV [7]. All these unique properties of SnO_2 have generated various applications for it, such as chemical and gas sensors, transparent conductive electrodes, super-capacitors, solar cells, and photocatalysts [8]. At the nanometric scale, SnO_2 exhibits extraordinary properties due to its high surface to volume ratio, which makes it a unique photocatalyst. During the last decades, a large number of chemical and physical methods have been developed for the synthesis of tin dioxide (SnO_2) nanoparticles (NPs) [9]. However, they require high temperature, a lot of energy, have a high operating cost, and use a large amount of organic solvents that are toxic and dangerous to the environment. Due to the negative impact of these methods against nature, there is a need to replace them with simple, inexpensive, biocompatible, and non-toxic methods [10].

* Corresponding author.
** Corresponding author.
E-mail addresses: andres.castro@uas.edu.mx (A. Castro-Beltrán), pluque@uabc.edu.mx (P.A. Luque).

https://doi.org/10.1016/j.molstruc.2019.07.052
0022-2860/

Recently, green synthesis has attracted the attention of many researchers because it is friendly to the environment and it makes use of non-hazardous solvents, which are usually plant extracts. These extracts come from the leaves, fruits, rinds, barks, seeds, and roots, as they have large amounts of polyphenols, flavonoids, proteins, and/or sugars, which act as both reducing and stabilizing agents at the same time [11]. In this work, we make use of tomatoes for the nanoparticle synthesis as it is one of the most important vegetables in the world due to its high consumption, availability throughout the year, and its high content of antioxidants, which can serve as reducing agents on precursor metal salts [12]. Its nutritional and functional components include the presence of phenolic compounds, carotenoids, ascorbic acid (vitamin C), vitamin E, folic acid, and flavonoids [13]; the latter are found in a high percentage, particularly in the skin (husk or peel) of the tomato [14]. Having said all of the above and due to its richness in phytochemicals that can act as reducing agents, this fruit is positioned as a suitable candidate for the biosynthesis of materials via green chemistry methods. Some authors have reported the use of extracts of *Lycopersicon esculentum* to obtain different types of NPs, such as silver [15], gold [16], copper [17], copper oxide [18], iron oxide [19], and zinc oxide [20]. However, up to now there have been very few studies on the biosynthesis of SnO_2 NPs; for example, *Calotropis gigantea* leaf extract of was obtained at 100 °C for its use in synthesis through microwaves and calcination [21], while Srivastava et al. have opted for the use of Gram-negative bacteria *Erwinia herbicola*. Both teams used their obtained samples in photocatalytic dye degradation [22]. Therefore, the study on the green synthesis of SnO_2 NPs using extracts of *Lycopersicon esculentum* for use in the degradation of methylene blue (MB) has not yet been reported. In this work, we study the biosynthesis of SnO_2, varying the concentration of *Lycopersicon esculentum* extract, for its evaluation in the photocatalytic MB degradation.

2. Experimental

2.1. Materials

For the development of this work, the following materials were used: tin chloride ($SnCl_2{\cdot}2H_2O$) was used as a tin precursor, purchased from Sumilab; *Lycopersicon esculentum* (tomato) peels for the reducing agent; and deionized water as the synthesis medium.

2.2. Preparation of peel extracts

Different concentrations of *Lycopersicon esculentum* peel extracts were used, obtained with 1%, 2% and 4% (weight-volume) of the husks in an aqueous medium. For the extraction process of the photochemical agents of the tomato peel, the different concentrations of peels are placed in agitation for 2 h. The mixtures are later placed in a water bath at 90 °C for an hour, after which they are filtered, to obtain the pure extracts, which are used as a reducing agent in the synthesis.

2.3. Synthesis of SnO_2 NPs

For the synthesis process of SnO_2 NPs, 2 g of tin chloride ($SnCl_2{\cdot}2H_2O$) are added as a tin precursor in 42 ml of the different *Lycopersicon esculentum* extracts and left to stir until completely dissolved; obtaining three different samples for 1%, 2% and 4% peel extract, respectively. After this, the samples are placed in a water bath at 60 °C until they have a pasty consistency, and are then calcined at 400 °C for 60 min. At the end of the process, a dry dark gray material is obtained for each sample, which is pulverized for its application.

2.4. Characterization

2.4.1. X-ray diffraction (XRD)

To understand the crystal structure of the samples, the studies were carried out using an X-ray diffractometer (D2-Phaser, Bruker). The diffractometer was operated at 30 kV, 10 mA in a range of 10–80° 2θ, with a step size of 0.02°, and a counting time of 1 s/step. The obtained SnO_2 powders were ground in an agate mortar and loaded onto a support, which is placed on a quartz plate for exposure to Cu K-α radiation, with a wavelength of 1.5406 Å.

2.4.2. Fourier-transform infrared spectroscopy (FTIR)

To know what functional groups are present in the materials, the FT-IR spectra were obtained by manipulating a Spectrum Two infrared spectrophotometer (PerkinElmer) with a direct detector in transmittance mode and a resolution of 0.5 cm^{-1}. The samples of SnO_2 powder, previously ground in an agate mortar, were placed in contact with horizontal attenuated total reflectance (UATR) at room temperature (20 °C), and the spectra were obtained using Spectrum in Software Lab, version 6.0.

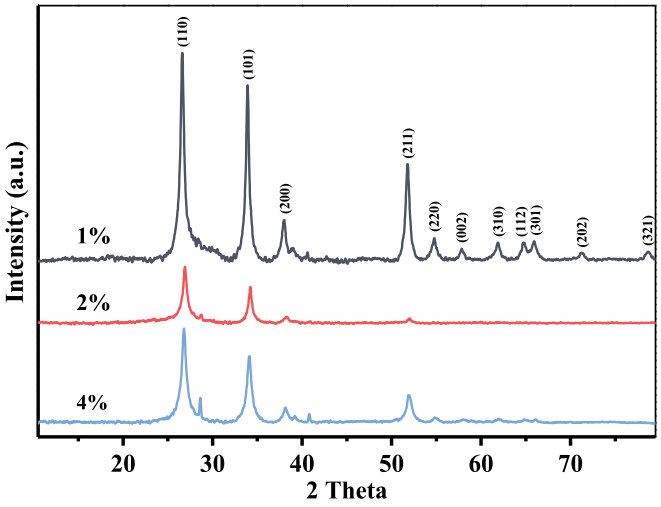

Fig. 1. XRD pattern of the SnO_2 samples.

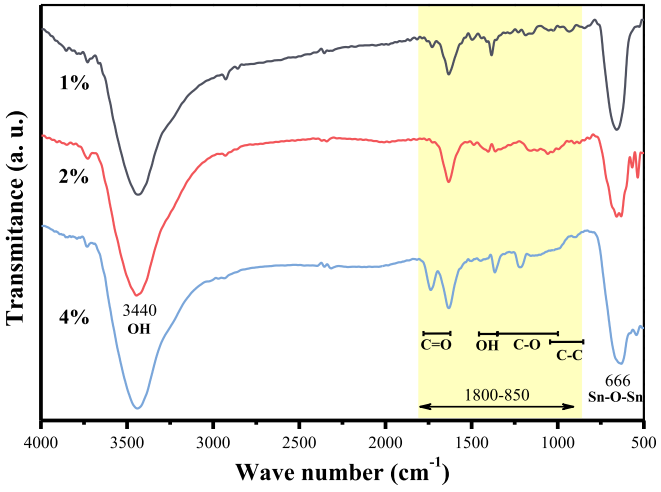

Fig. 2. FTIR spectra of the SnO_2 samples.

2.4.3. High-resolution transmission electron microscopy (HRTEM) and selective area electron diffraction (SAED)

For the study of the morphology of the NPs, the samples were analyzed in a JEM-2100 Transmission Electron Microscope with a LaB_6 filament and operated at an accelerating voltage of 200 kV. For analysis, biosynthesized SnO_2 samples are dispersed in isopropyl alcohol by ultrasound. Some of the suspension is immediately placed on a copper grid coated with a carbon film, then dry under ambient conditions and examined under the transmission electron microscope.

2.4.4. Ultra violet-to-visible spectroscopy (UV–Vis)

Used to study the band gap and the catalytic activity during the MB degradation, the UV–Vis analysis of these samples, a sweep of the UV–Vis wavelength from 190 to 700 nm was performed on a PerkinElmer UV/VIS Lamda 365 spectrophotometer. For the Band gap analysis, 50 mg of SnO_2 nanoparticles were suspended in 5 ml of water for each of the samples, forming aqueous solutions that were ultrasonicated for 180 s, improving dispersion.

2.5. Photocatalytic activity

The photocatalytic activity of the synthesized SnO_2 NPs was

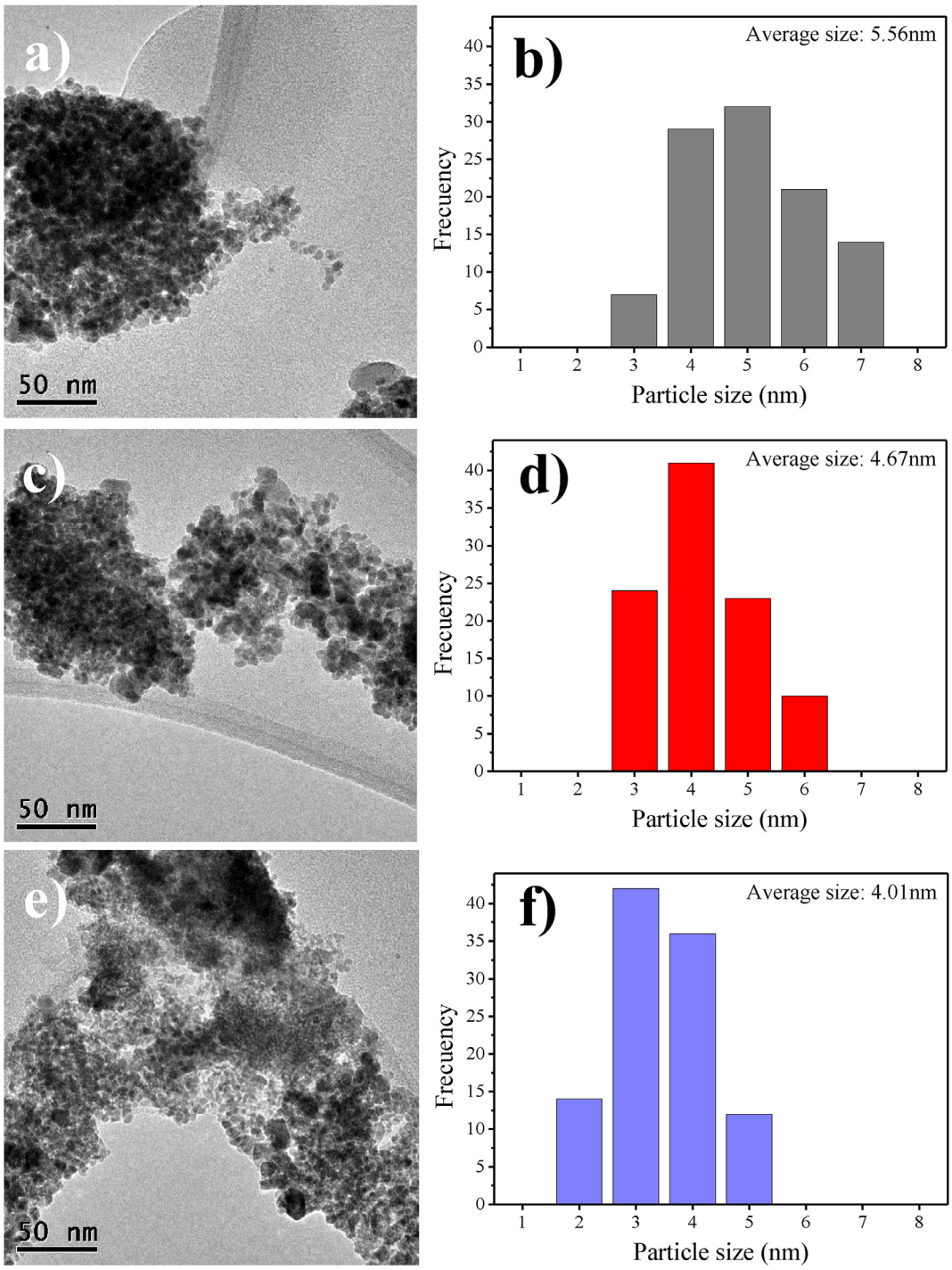

Fig. 3. TEM (a, c, & e) & Size distribution (d, b, & f) of the different SnO_2 samples, along with their respective size averages.

analyzed for the degradation of MB, as a contaminant, under UV irradiation. The photocatalytic experiment was carried out in a closed, stainless steel reactor containing a 10W Hg UV lamp at a dose of 18 mJ/cm^2. Before irradiating the solution with UV light, 100 mg of the photocatalyst samples are added in to 100 ml of a MB solution (15 ppm) at neutral pH, and stirred magnetically for 30 min in the dark to guarantee an adsorption-desorption equilibrium of the MB at the start of the reaction. After irradiating the solution with UV light, 2 mL aliquots were taken at 10 min time intervals for 2 h. The concentration of MB was determined by measuring the intensity of absorption through a UV–Vis spectrophotometer in a range of 400–800 nm wavelengths.

3. Results and discussion

3.1. XRD

Fig. 1 shows the XRD patterns of all biosynthesized SnO_2 samples. The peaks with 2θ values at 26.5°, 34°, 37.9°, 51.7°, 54.4°, 57.7°, 61.7°, 64.8°, 71.3° and 78.5° are associated with the (110), (101), (200), (211), (220), (002), (310), (301), (202) and (222) planes, respectively, indicating the formation of SnO_2 with a tetragonal structure in the rutile phase, according to the JCPDS file No. 41-1445 [23,24]. Yet, in the SnO_2 samples with increased amounts of extract (2 and 4%), the XRD patterns presented fewer peaks, which indicates that the materials are becoming amorphous. The low

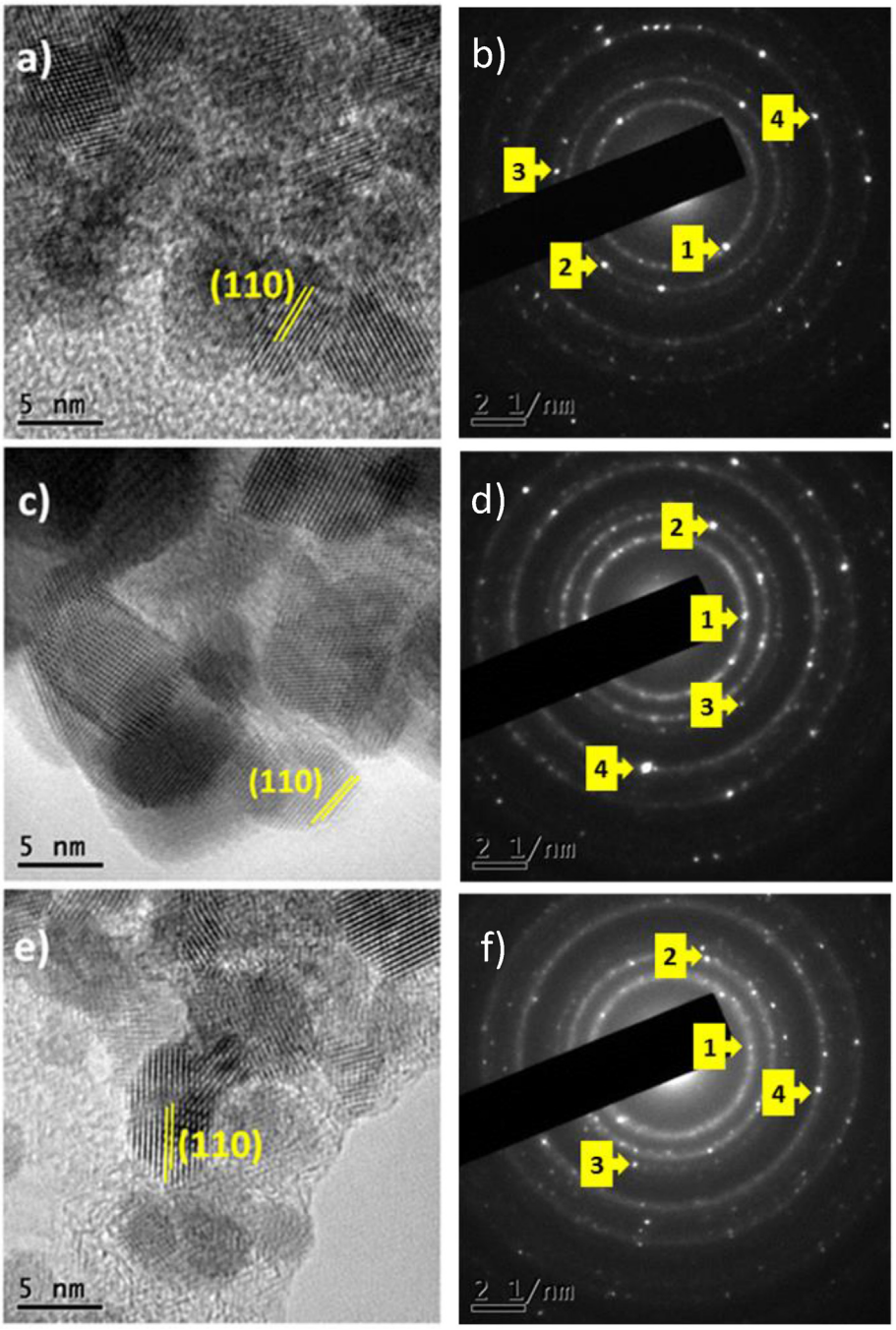

Fig. 4. HRTEM (a, c, & e) & SAED (b, d, & f) studies of synthesized samples showing the interplanar distance and diffraction ring of each sample.

intensity reflections, observed in the diffractogram at a 2θ value of 28.6° and 40.47°, can be attributed to the KCl phase due to the large amount of K present in the *Lycopersicon esculentum* [25,26], and to the Chlorine ions of the tin precursor.

3.2. FTIR

In Fig. 2, the infrared spectra can be observed for all three samples (1%, 2% and 4%). For the three spectra, similar bands are observed. A band at 3440 cm^{-1} due to the stretching vibrations of the OH bond [27]. Another band is observed at 1629 cm^{-1} due to the $SnCl_2$ molecules that managed to hydrolyze in the process but failed to crystallize [28]. In addition, a set of bands is observed in the range of 1800 cm^{-1} to 850 cm^{-1} that is attributed to the vibrations of the OH, C-O, C═O and C-C bonds present due to the organic compounds in the *Lycopersicon esculentum* extract [29–31]. Finally, a 666 cm^{-1} band is observed attributed to the Sn-O-Sn bond vibration that is characteristic of SnO_2 [32]. These results indicate both the presence of the organic material of the extract, as well as the successful formation of SnO_2 for all three samples.

3.3. Morphological study

The TEM analysis of the biosynthesized samples is observed in Fig. 3. In the analysis, a predominant morphology with a quasi-spherical form was found for all of the NP samples, with only some agglomerates (Fig. 3a, c and e). The main effect observed was the decrease in the size of the NPs as the percentage of extract used in the biosynthesis of SnO_2 was increased. Average sizes of 5.56 nm, 4.67 nm and 4.01 nm were obtained for the 1%, 2% and 4% samples, respectively (Fig. 3b, d and f). The interplanar distance for all the samples was also obtained (Fig. 4a, c and e), which was of 0.33 nm, corresponding to the (110) plane of the SnO_2 [33]. This coincides with what was observed in the XRD analysis. Fig. 4b, d, and f show the SAED patterns, which revealed the diffraction rings 1, 2, 3 and 4, corresponding to reflections (110), (101), (200) and (211). These can be related to the tetragonal structure of the SnO_2. The size averages achieved by all the samples was within the ideal margin to be applied in photocatalysis [34].

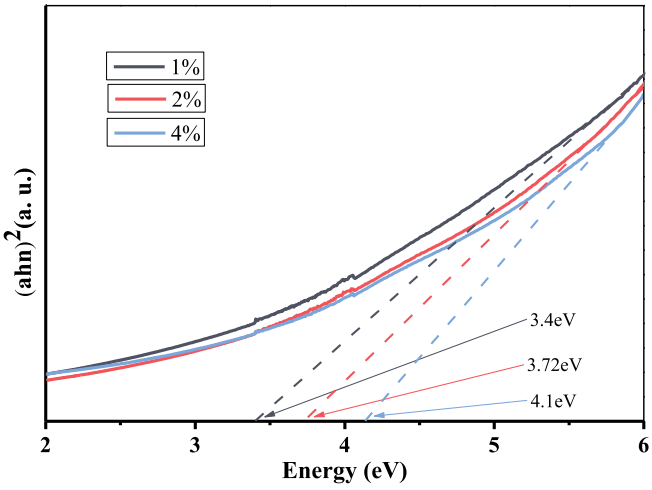

Fig. 5. SnO_2 NPs sample band gaps.

3.4. Band gap

The samples were analyzed via UV–Vis and their band gaps were determined using the TAUC model [35], as shown in Fig. 5. Values of 3.4, 3.7 and 4.1 eV were found for the 1%, 2% and 4% samples, respectively. The variation of the band gap values is directly associated with the decrease in the size of the NPs (see Fig. 4) due to the effects of quantum confinement [36]. It can also be attributed to the presence of the extract in the samples, which affects the interactions of the electrons between the valence band and the conduction band. It should be mentioned that the values obtained are close to those of commercially bought bulk SnO_2, which suggests that the synthesized materials can be used in photocatalytic applications [37].

3.5. Catalytic activity

Fig. 6 shows the photocatalytic degradation of the MB under UV irradiation, as well as the degradation rate constants (k) of the biosynthesized SnO_2 NPs. Fig. 6a shows that as the percentage of *Lycopersicon esculentum* extract increases, MB adsorption increases. This is likely because the extract is functionalized on the surface of SnO_2, which has an affinity for the MB molecules, producing an increase in photodegradation efficiency. After 120 min of irradiation with UV light, the samples achieve 67%, 85%, and 99% degradation for the 1%, 2% and 4% samples, respectively. The sample with the highest photocatalytic performance is the sample with 4% extract, due to the large amount of MB molecules absorbed (60%),

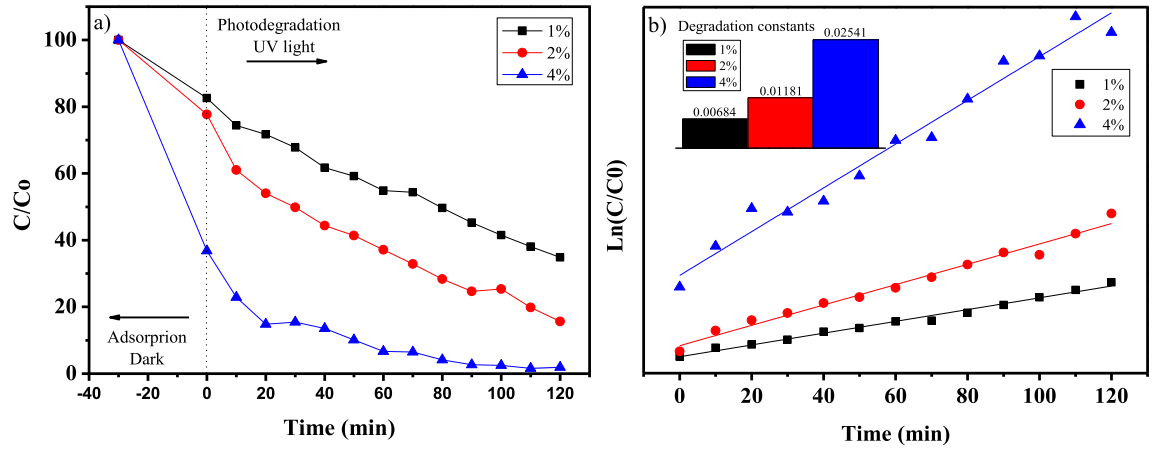

Fig. 6. a) Photocatalytic degradation of MB, b) kinetic plot of Ln(C/C_0) versus irradiation time and rate constant k values for the photodegradation of MB using 1%, 2% and 4% of tomato extract in the biosynthesis of SnO_2 nanoparticles.

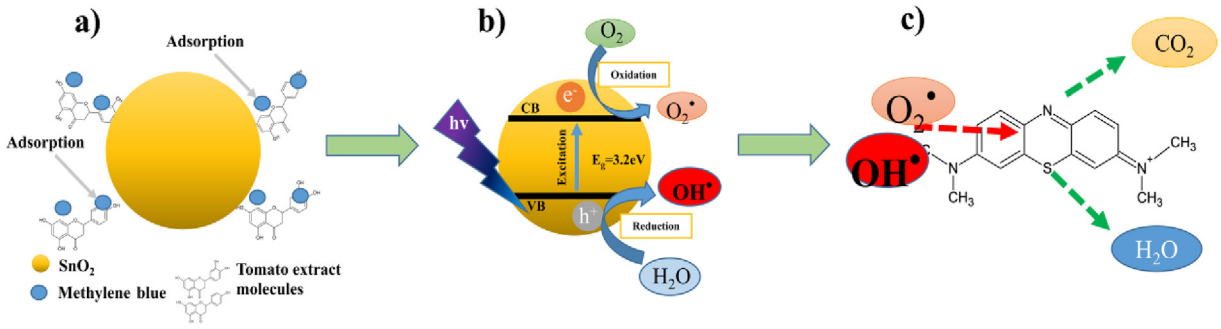

Fig. 7. Schematic of the photocatalytic process of SnO_2 nanoparticles in three stages: (a) adsorption, (b) generation of oxidative species and (c) MB degradation.

and also because it has the smallest average size. It should be mentioned that these results are very good, since other studies have reported a degradation of only 93% in 120 min using other extracts in the biosynthesis [38]. The degradation of MB with SnO_2 nanoparticles mainly follows pseudo first-order kinetics and it is calculated with the following equation [39]:

$$\ln(C/C_0) = kKt = kt$$

where k is the reaction rate constant, K is the adsorption coefficient of the reactant and t is the time. A plot of $\ln(C/C_0)$ versus time represents a straight line; the slope equals the apparent first-order rate constant (k). The MB photodegradation kinetics of the SnO_2 nanoparticles was studied and the results are shown in Fig. 6b. According to the pseudo-first-order rate equation, the rate constant (k) was determined used the plot of $\ln(C/C_0)$ as a function of irradiation time, obtaining approximate values of 0.00684, 0.01181 and 0.02541 for the 1%, 2% and 4% samples, respectively.

3.6. Photocatalytic degradation mechanism

Fig. 7 shows a schematic representation of the photocatalytic degradation process of MB, using SnO_2 as photocatalyst and UV light as irradiation source. The degradation process can be divided into three stages: (1) adsorption, (2) generation of oxidative species, and (3) MB degradation. The SnO_2 nanoparticles showed an excellent MB molecule adsorption capacity (see Fig. 6) due to the π-π interactions between the MB and the aromatic rings present in the tomato extract. The adsorption enriched the concentration of MB molecules over the extract, placing the MB closer to the photocatalytic surface of the SnO_2, which is a pre-requisite to enhance photocatalytic activity (Fig. 7a). The generation of oxidative species starts with the irradiation of the SnO_2 with UV light, producing electrons in the conduction band and gaps in the valence band (known as the photo-excitation process), which generates electron-hole pairs [40]. These electrons interact with the dissolved oxygen (O_2) and photo-oxidize it to generate superoxide radicals (O_2•), while the voids photo-reduce water molecules (H_2O) generating hydroxyl radicals (OH•). Both are highly oxidizing species (Fig. 7b). Finally, the MB degradation start when the O_2• and OH• radicals degrade the MB molecules, producing H_2O and carbon dioxide (CO_2) as byproducts of the reaction (Fig. 7c) [41].

4. Conclusions

This work details the green chemistry synthesis and characterization of SnO_2 NPs synthesized using *Lycopersicon esculentum* extract. The crystal sizes and homogeneity of the SnO_2 NPs was influenced by the amount of peel (weight-volume) in the extract used during the synthesis. The photocatalytic activity presented a MB degradation of 100% within 120 min; a better degradation ratio than that of NPs from others studies that use different synthesis methods, and better than commercially bought bulk SnO_2 NPs. This synthesis method is a simple, non-toxic way of obtaining polycrystalline SnO_2 NPs.

Acknowledgments

The authors thank the support of CONACYT projects numbered 4940 and 295075.

References

[1] S.M. Hosseinpour-Mashkani, A. Sobhani-Nasab, Green synthesis and characterization of $NaEuTi_2O_6$ Nanoparticles and its photocatalyst application, J. Mater. Sci. Mater. Electron. 28 (2017) 4345–4350.
[2] A. Safavi, S. Momeni, Highly efficient degradation of azo dyes by palladium/hydroxyapatite/Fe_3O_4 nanocatalyst, J. Hazard Mater. 201 (2012) 125–131.
[3] B.C. Ventura-Camargo, M.A. Marin-Morales, Azo dyes: Characterization and toxicity– a review, Text. Light Ind. Sci. Technol. 2 (2013) 85–103.
[4] V. Katheresan, J. Kansedo, S.Y. Lau, Efficiency of various recent wastewater dye removal methods: A review, J. Environ. Chem. Eng. 6 (2018) 4676–4697.
[5] S.P. Kim, M.Y. Choi, H.C. Choi, Photocatalytic activity of SnO_2 nanoparticles in methylene blue degradation, Mater. Res. Bull. 74 (2016) 85–89.
[6] H. Wang, L. Zhang, Z. Chen, J. Hu, S. Li, Z. Wang, X. Wang, Semiconductor heterojunction photocatalysts: Design, construction and photocatalytic performances, Chem. Soc. Rev. 43 (2014) 5234–5244.
[7] R. Khan, Y. Yuan, Z. Iqbal, J. Yang, W. Wang, Z. Ye, J. Lu, Variation of structural, optical, dielectric and magnetic properties of SnO_2 nanoparticles, J. Mater. Sci. Mater. Electron. 28 (2017) 4625–4636.
[8] H. Wang, A.L. Rogach, Hierarchical SnO_2 nanostructures: Recent advances in design, synthesis and applications, Chem. Mater. 26 (2013) 123–133.
[9] E.T. Selvi, S.M. Sundar, Effect of size on structural, optical and magnetic properties of SnO_2 nanoparticles, Mater. Res. Express 4 (2017), 075903.
[10] M. Yadi, E. Mostafavi, B. Saleh, S. Davaran, I. Aliyeva, R. Khalilov, M. Milani, Current developments in green synthesis of metallic nanoparticles using plant extracts: A review, Artif. cells, Nanomed. Biotechnol 10 (2018) 1–8.
[11] A.K. Mittal, Y. Chisti, U.C. Banerjee, Synthesis of metallic nanoparticles using plant extracts, Biotechnol. Adv. 31 (2013) 346–356.
[12] E. Elbadrawy, A. Sello, Evaluation of nutritional value and antioxidant activity of tomato peel extracts, Arab J. Chem. 9 (2016) S1010–S1018.
[13] W. Klunklin, G. Savage, Effect on quality characteristics of tomatoes grown under well-watered and drought stress conditions, Foods 6 (8) (2017) 56.
[14] R.K. Toor, C.E. Lister, G.P. Savage, Antioxidant activities of New Zealand-grown tomatoes, Int. J. Food Sci. Nutr. 56 (8) (2005) 597–605.
[15] A. Bhattacharyya, R. Prasad, A.A. Buhroo, P. Duraisamy, I. Yousuf, M. Umadevi, M.R. Bindhu, M. Govindarajan, A.L. Khanday, One-pot fabrication and characterization of silver nanoparticles using *Solanum lycopersicum*: An eco-friendly and potent control tool against rose aphid, *Macrosiphum rosae*, J. Nanosci. 2016 (2016). ID4679410.
[16] M. Pattanayak, P.L. Nayak, Green synthesis of gold nanoparticles using *Solanus lycopersicum* (TOMATO) aqueous extract, World J. Nano. Sci. Technol. 3 (2014) 74–80.
[17] M. Batoool, B. Masood, Green synthesis of copper nanoparticles using *Solanum lycopersicum* (Tomato Aqueous Extract) and study characterization, J. Nanosci. Nanotechnol. 1 (2017) 1–5.
[18] V. Dandapani, V. Bhuvaneshwari, D. Bharathi, B.P. Sheetal, Antibacterial and photocatalytic activity of copper oxide nanoparticles synthesized using *Solanum lycopersicum* leaf extract, Mater. Res. Express 5 (2018), 085403.
[19] T. Pavani, K. Venkateswara Rao, C.S. Chakra, Y.T. Prabhu, Synthesis and characterization of γ-ferric oxide nanoparticles and their effect on *Solanum*

lycopersicum, Environ. Sci. Pollut. Res. 23 (2016) 9373–9380.
[20] C.A. Soto-Robles, O.J. Nava, A.R. Vilchis-Nestor, A. Castro-Beltrán, C.M. Gómez-Gutiérrez, E. Lugo-Medina, A. Olivas, P.A. Luque, Biosynthesized zinc oxide using *Lycopersicon esculentum* peel extract for methylene blue degradation, J. Mater. Sci. Mater. Electron. 29 (2018) 3722–3729.
[21] T.T. Bhosale, H.M. Shinde, N.L. Gavade, S.B. Babar, V.V. Gawade, S.R. Sabale, R.J. Kamble, B.S. Shirke, K.M. Garadkar, Biosynthesis of SnO_2 nanoparticles by aqueous leaf extract of *Calotropis gigantean* for photocatalytic applications, J. Mater. Sci. Mater. Electron. 29 (2018) 6826–6834.
[22] N. Srivastava, M. Mukhopadhyay, Biosynthesis of SnO_2 nanoparticles using bacterium *Erwinia herbicola* and their photocatalytic activity for degradation of dyes, Ind. Eng. Chem. Res. 53 (2014) 13971–13979.
[23] S. Sathishkumar, M. Parthibavarman, V. Sharmila, M. Karthik, A facile and one step synthesis of large surface area SnO_2 nanorods and its photocatalytic activity, J. Mater. Sci. Mater. Electron. 28 (2017) 8192–8196.
[24] K. Saravanakumar, V. Muthuraj, Fabrication of sphere like plasmonic Ag/SnO_2 photocatalyst for the degradation of phenol, Optik 131 (2017) 754–763.
[25] A.K. Swain, D. Bahadur, Facile synthesis of twisted graphene solution from graphite-KCl, RSC Adv. 3 (42) (2013) 19243–19246.
[26] D. Erba, M.C. Casiraghi, A. Ribas-Agustí, R. Cáceres, O. Marfà, M. Castellari, Nutritional value of tomatoes (*Solanum lycopersicum* L.) grown in greenhouse by different agronomic techniques, J. Food Compos. Anal. 31 (2) (2013) 245–251.
[27] N. Selvi, S. Sankar, K. Dinakaran, Interfacial effect on the structural and optical properties of pure SnO_2 and dual shells (ZnO; SiO_2) coated SnO_2 core-shell nanospheres for optoelectronic applications, Superlattice Microstruct. 76 (2014) 277–287.
[28] R. Malik, V.K. Tomer, S. Duhan, S.P. Nehra, P.S. Rana, One-pot hydrothermal synthesis of porous SnO_2 nanostructures for photocatalytic degradation of organic pollutants, Energy Environ. Focus 4 (2015) 340–345.
[29] E. Sabio, A. Álvarez-Murillo, S. Román, B. Ledesma, Conversion of tomato-peel waste into solid fuel by hydrothermal carbonization: Influence of the processing variables, Waste Manag. 47 (2016) 122–132.
[30] G. Toscano, A. Pizzi, E. Foppa Pedretti, G. Rossini, G. Ciceri, G. Martignon, D. Duca, Torrefaction of tomato industry residues, Fuel 143 (2015) 89–97.
[31] S. Vermeir, K. Beullens, P. Mészáros, E. Polshin, B.M. Nicolaï, J. Lammertyn, Sequential injection ATR-FTIR spectroscopy for taste analysis in tomato, Sens. Actuators B Chem. 137 (2) (2009) 715–721.
[32] P. Chand, Effect of pH values on the structural, optical and electrical properties of SnO_2 nanostructures, Optik 181 (2019) 768–778.
[33] V. Kamble, A.M. Umarji, Achieving selectivity from the synergistic effect of Cr and Pt activated SnO_2 thin film Gas Sensors, Sens. Actuators B Chem. 236 (2016) 208–217.
[34] A.M. Al-Hamdi, U. Rinner, M. Sillanpää, Tin dioxide as a photocatalyst for water treatment: A review, Process Saf. Environ. Prot. 107 (2017) 190–205.
[35] B.D. Viezbicke, S. Patel, B.E. Davis, D.P. Birnie, Evaluation of the Tauc method for optical absorption edge determination: ZnO thin films as a model system, Phys. Status Solidi B 252 (2015) 1700–1710.
[36] S. Jagpreet, K. Sukhmeen, K. Gaganpreet, B. Soumen, R. Mohit, Biogenic ZnO nanoparticles: A study of blue shift of optical band gap and photocatalytic degradation of reactive yellow 186 dye under direct sunlight, Green Process. Synth. 8 (2019) 272–280.
[37] J. Osuntokun, D.C. Onwudiwe, E.E. Ebenso, Biosynthesis and photocatalytic properties of SnO_2 nanoparticles prepared using aqueous extract of Cauliflower, J. Clust. Sci. 28 (2017) 1883–1896.
[38] R. Lei, H. Ni, R. Chen, B. Zhang, W. Zhan, Y. Li, Growth of Fe_2O_3/SnO_2 nanobelt arrays on iron foil for efficient photocatalytic degradation of methylene blue, Chem. Phys. Lett. 673 (2017) 1–6.
[39] I.K. Punithavathy, J.P. Richard, S.J. Jeyakumar, M. Jothibas, P. Praveen, Photodegradation of methyl violet dye using ZnO nanorods, J. Mater. Sci. Mater. Electron. 28 (2017) 2494–2501.
[40] J. Wang, C. Lu, X. Liu, Y. Wang, Z. Zhu, D. Meng, Synthesis of tin oxide (SnO & SnO_2) micro/nanostructures with novel distribution characteristic and superior photocatalytic performance, Mater. Des. 115 (2017) 103–111.
[41] M.A. Ahmed, M.F.A. Messih, E.F. El-Sherbeny, S.F. El-Hafez, A.M.M. Khalifa, Synthesis of metallic silver nanoparticles decorated mesoporous SnO_2 for removal of methylene blue dye by coupling adsorption and photocatalytic processes, J. Photochem. Photobiol., A 346 (2017) 77–88.